

# Charged grain boundaries reduce the open circuit voltage of polycrystalline solar cells – an analytic description

Benoit Gaury<sup>1,2</sup> and Paul M. Haney<sup>1</sup>

<sup>1</sup>*Center for Nanoscale Science and Technology, National Institute of Standards and Technology, Gaithersburg, MD 20899, USA*

<sup>2</sup>*Maryland NanoCenter, University of Maryland, College Park, MD 20742, USA*

(Dated: 27 March 2025)

Analytic expressions are presented for the dark current-voltage relation  $J(V)$  of a  $pn^+$  junction with charged columnar grain boundaries with high defect density. These expressions apply to non-depleted grains with sufficiently high bulk hole mobilities. The accuracy of the formulas is verified by direct comparison to numerical simulations. Numerical simulations further show that the dark  $J(V)$  can be used to determine the open circuit potential  $V_{oc}$  of an illuminated junction for a given short circuit current density  $J_{sc}$ . A precise relation between the grain boundary properties and  $V_{oc}$  is provided, advancing the understanding of the influence of grain boundaries on the efficiency of thin film polycrystalline photovoltaics like CdTe and Cu(In, Ga)Se<sub>2</sub>.

## I. INTRODUCTION

Despite decades of research, the role of grain boundaries in the photovoltaic behavior of polycrystalline solar cells remains an open question<sup>1,2</sup>. The high defect density of grain boundaries generally promotes recombination and reduces photovoltaic efficiency. However, thin film polycrystalline photovoltaics such as CdTe and Cu(In, Ga)Se<sub>2</sub> exhibit high efficiencies despite a large density of grain boundaries<sup>3,4</sup> (both materials' grain size is on the order of microns). The unexpected high efficiency of these materials demonstrates the need for a fuller understanding of grain boundary properties, and their influence on the charge current and recombination.

Numerous nanoscale measurements using electron beam induced current<sup>5-7</sup>, scanning Kelvin probe microscopy<sup>8-10</sup> and other techniques<sup>11-13</sup> have revealed that grain boundaries in these materials are positively charged (although previous work has also argued for negatively charged grain boundaries<sup>14</sup>). Interpretation of these measurements is often challenging due to extraneous factors, such as surface effects<sup>15</sup>. However, the information obtained from these measurements is sufficient to inform the construction of relevant models of grain boundaries. These models in turn provide critical feedback on the validity of the qualitative conclusions drawn from experiments.

The impact of charged grain boundaries on the photovoltaic efficiency has been studied using numerical simulations<sup>16-19</sup>, and to a lesser extent, analytic models<sup>20-22</sup>. These studies show that sufficiently large band bending at grain boundaries minimizes their impact on the short circuit current, but that grain boundaries always reduce the open circuit voltage  $V_{oc}$ . This is consistent with the observation that the  $V_{oc}$  of CdTe is far below its theoretical maximum, and is the metric for which the largest efficiency improvements are available<sup>3</sup>. This highlights the need for a quantitative understanding of grain boundaries on  $V_{oc}$ . Although simulations can provide insight, the nonlinearities of the system and the large number

of material parameters make it difficult to formulate a complete picture of the system using numerical modeling alone.

In this work we present analytical expressions for the dark current-voltage  $J(V)$  relation of a  $pn^+$  junction with positively charged, columnar grain boundaries. We find that grain boundaries contribute substantially to the dark current. Because the electrostatics around and at the grain boundary controls the grain boundary transport properties, but differs from the bulk  $pn$  junction, it requires new analysis. Our analysis applies for grains which are not fully depleted and for materials with sufficiently high hole mobility. We show that the dark  $J(V)$  approximately determines  $V_{oc}$  and provides a closed form description for how charged grain boundaries reduce  $V_{oc}$ . Our analytical results follow from studying a large number of numerical simulations, formulating a physical picture of the electron and hole currents and recombination, and translating this picture into a simplified effective model which describes the essential features of the full simulation. We verify the accuracy of the model by direct comparison with the simulations.

The paper is organized as follows: in Sec. II we describe the physical model and the assumptions we use in our analysis. In Sec. III we present the derivation of the dark  $J(V)$  relation. We find the system response depends qualitatively on the magnitude of the current: for lower currents, there is uniform recombination along the length of the grain boundary, while for higher currents, recombination is peaked at the grain boundary in the  $pn$  junction depletion region. The  $J(V)$  relations for these cases are summarized in Table I. Similar results have been obtained in previous works on this problem<sup>20,22</sup>, however some of the relations we present are new. In Sec. IV we derive the bulk recombination current from the grain interior and  $pn$  junction depletion region. In Sec. V we show numerically that the dark  $J(V)$  yields a good estimate of  $V_{oc}$ . Finally we discuss the implications of our analysis for understanding how grain boundaries impact photovoltaic efficiency and measurements of these mate-

rials.

## II. PHYSICAL MODEL OF THE GRAIN BOUNDARY AND RESTRICTIONS

The model system, depicted in Fig. 1(a), is a  $pn^+$  junction of width  $d = 5 \mu\text{m}$  and length  $L = 3 \mu\text{m}$  with a single grain boundary perpendicular to the junction. We use selective contacts so that the hole (electron) current vanishes at  $x = 0$  ( $x = L$ ). We use periodic boundary conditions in the  $y$ -direction so that the system constitutes a closed grain. Motivated by experimental evidence of charged grain boundaries as discussed in introduction, we consider a two-dimensional model of a positively charged grain boundary. The response of the system to this positive charge is to develop an electric field surrounding the grain boundary which attracts electrons and screens the grain boundary charge. This results in band bending around the grain boundary and the formation of a built-in potential  $V_{GB}$  across it, as seen in Fig. 1(b). Experiments on CdTe indicate that grain boundary band bending is large enough to induce type inversion, so that electrons are majority carriers at the grain boundary core<sup>7</sup>. We therefore restrict our attention to inverted grain boundaries.

The grain boundary is readily modeled as a 2-dimensional plane with an increased concentration of defect states. The grain boundary charge density from a single defect energy level reads<sup>17</sup>

$$Q_{GB} = q \frac{\rho_{GB}}{2} (1 - 2f_{GB}) \quad (1)$$

where  $\rho_{GB}$  is the 2D defect density of the grain boundary and  $q$  is the absolute value of the electron charge. The occupancy of the defect level  $f_{GB}$  is given by<sup>23</sup>

$$f_{GB} = \frac{S_n n_{GB} + S_p \bar{p}_{GB}}{S_n (n_{GB} + \bar{n}_{GB}) + S_p (p_{GB} + \bar{p}_{GB})}, \quad (2)$$

where  $S_n$ ,  $S_p$  are recombination velocity parameters for electrons and holes respectively, and  $\bar{n}_{GB}$  and  $\bar{p}_{GB}$  are

$$\bar{n}_{GB} = N_C e^{(-E_g + E_{GB})/k_B T} \quad (3)$$

$$\bar{p}_{GB} = N_V e^{-E_{GB}/k_B T} \quad (4)$$

where  $E_{GB}$  is the grain boundary defect energy level calculated from the valence band edge,  $N_C$  ( $N_V$ ) is the conduction (valence) band effective density of states,  $E_g$  is the material bandgap,  $k_B$  is the Boltzmann constant and  $T$  is the temperature.

We consider large grain boundary defect densities, such that the Fermi level  $E_F$  is pinned at  $E_{GB}$  (see Fig. 1(b)). In Appendix A we show that the density of defects required for Fermi level pinning must exceed  $\rho_{GB}^{\text{crit}}$ , given by

$$\rho_{GB}^{\text{crit}} = \frac{2}{q} \left( \frac{e+1}{e-1} \right) \sqrt{8q\epsilon N_A (E_{GB} - E_F)}. \quad (5)$$

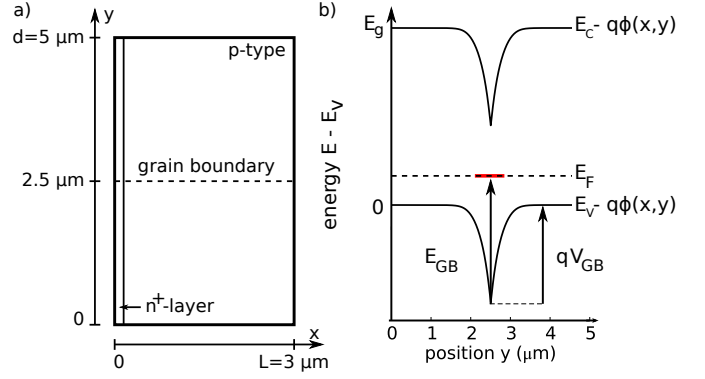


FIG. 1. (a) 2D model system of a  $pn^+$  junction containing a grain boundary. (b) Band structure in the neutral region of the  $p$ -doped semiconductor. The dashed line is the thermal equilibrium Fermi level  $E_F$ , and the grain boundary defect energy level is indicated by the short red line.  $E_C$  and  $E_V$  are the conduction and valence band edges,  $E_g$  is the material bandgap energy,  $E_{GB}$  is the distance between the valence band edge and the grain boundary defect energy level,  $V_{GB}$  is the grain boundary built-in potential, and  $\phi$  is the electrostatic potential. We take the energy reference at the valence band edge in the bulk of the neutral region.

For material parameters typical of CdTe,  $\rho_{GB}^{\text{crit}}$  is on the order of  $10^{12} \text{ cm}^{-2}$ . Defining  $V_{GB}^0$  as the equilibrium potential difference between the grain boundary and bulk of the neutral region, then assuming  $\rho_{GB} > \rho_{GB}^{\text{crit}}$  leads to

$$qV_{GB}^0 \approx E_{GB} - E_F. \quad (6)$$

The depletion region width surrounding the grain boundary is  $W_{GB} = \sqrt{2\epsilon V_{GB}^0 / (qN_A)}$ . We restrict this work to grain sizes  $d$  which are greater than  $2W_{GB}$ , so that the grain is not fully depleted. For a doping density  $10^{15} \text{ cm}^{-3}$  this requirement implies  $d > 2 \mu\text{m}$ . We leave the case of fully depleted grains for future study.

Finally, we assume that the hole quasi-Fermi level is approximately flat. In the analysis below we indicate precisely where this assumption is invoked, and provide a criterion for its validity. We find that for typical material parameters of CdTe, this assumption is generally valid.

## III. GRAIN BOUNDARY DARK CURRENT

In this section we derive analytical expressions for the dark current originating from the grain boundary recombination. The general expression of the grain boundary recombination current density reads

$$J_{GB}(V) = \frac{1}{d} \int_0^{L_{GB}} dx R_{GB}(x), \quad (7)$$

where  $L_{GB}$  is the length of the grain boundary.  $R_{GB}$  is the recombination at the grain boundary and has the

Schockley-Read-Hall form

$$R_{\text{GB}} = \frac{S_n S_p (n_{\text{GB}} p_{\text{GB}} - n_i^2)}{S_n (n_{\text{GB}} + \bar{n}_{\text{GB}}) + S_p (p_{\text{GB}} + \bar{p}_{\text{GB}})}. \quad (8)$$

$S_n$ ,  $S_p$  and  $\rho_{\text{GB}}$  are related to the electron and hole capture cross sections  $\sigma_n$ ,  $\sigma_p$  of the grain boundary defect level by  $S_{n,p} = \sigma_{n,p} v_t \rho_{\text{GB}}$ , where  $v_t$  is the thermal velocity. In this work we vary  $S_{n,p}$ ; for a fixed  $\rho_{\text{GB}}$  this corresponds to varying  $\sigma_{n,p}$ .

We find that the appropriate analysis of the grain boundary recombination depends on the relative electron and hole densities at the grain boundary. The relevant cases are  $S_n n_{\text{GB}} \gg S_p p_{\text{GB}}$  and  $S_n n_{\text{GB}} \approx S_p p_{\text{GB}}$ . In both cases, the recombination is determined by the hole density at the grain boundary. We will assume that the hole quasi-Fermi level is constant, so that the hole density is determined solely by the electrostatic potential. Therefore in both cases our procedure is to:

1. find an expression for the electrostatic potential at the grain boundary,
2. determine the hole density,
3. use the hole density to compute the grain boundary recombination.

We find two distinct regimes: for lower currents, the recombination occurs uniformly throughout the length of the grain boundary, while for higher currents the recombination is peaked at the grain boundary in the  $pn$  junction depletion region.

#### A. Grain boundary recombination for $S_n n_{\text{GB}} \gg S_p p_{\text{GB}}$

In this section we assume that  $S_n n_{\text{GB}} \gg S_p p_{\text{GB}}$ . In the grain interior of the neutral  $p$ -type region, the electron quasi-Fermi level  $E_{F_n}$  increases linearly with the applied voltage  $V$  (see Fig. 2(d)). We assume that  $E_{F_n}$  is approximately flat across the grain boundary, so that everywhere outside the  $pn$  junction depletion region,  $E_{F_n} = E_F + qV$ . This shift in  $E_{F_n}$  leads to a nonequilibrium electron density in the  $p$ -type region induced by the applied voltage.

Next, we consider how this nonequilibrium electron density impacts  $V_{\text{GB}}$ . When  $S_n n_{\text{GB}} \gg S_p p_{\text{GB}}$ , the occupation and charge of the grain boundary defect level is determined solely by the electron density  $n_{\text{GB}}$  at the grain boundary (see Eq. (2)). Therefore under nonequilibrium conditions, the Fermi level pinning assumption described in Sec. II generalizes to *electron* quasi-Fermi level pinning. The corresponding expression for  $V_{\text{GB}}$  is then

$$\begin{aligned} qV_{\text{GB}} &\approx E_{\text{GB}} - E_{F_n} \\ &= E_{\text{GB}} - E_F - qV \\ &= q(V_{\text{GB}}^0 - V). \end{aligned} \quad (9)$$

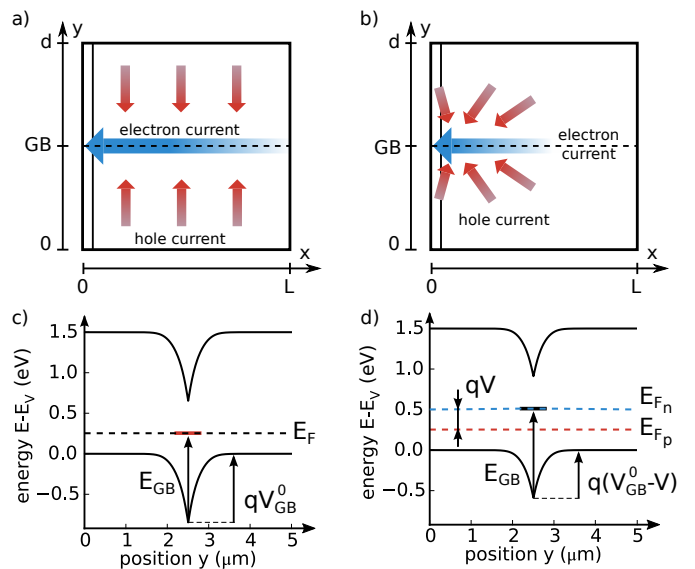


FIG. 2. (a) Schematic of the electron and hole currents in the linear regime. (b) Schematic of the electron and hole currents in the hotpost regime. (c) Band diagram of our model system at thermal equilibrium. (d) Band diagram in the neutral region under applied bias  $V$ , corresponding to situation (a). The dashed lines correspond to the quasi-Fermi levels  $E_{F_n}$  (upper, blue) and  $E_{F_p}$  (lower, red).  $V$  is the applied voltage.

Equation (9) shows that the potential difference between grain boundary and neutral bulk decreases linearly with  $V$ . The physical picture is that the accumulation of nonequilibrium electrons partially neutralizes the positively charged grain boundary, reducing the electrostatic hole barrier surrounding the grain boundary. The reduction of this barrier results in a flow of hole current towards the grain boundary, depicted schematically in Fig. 2(a). The holes recombine at the grain boundary core, generating an electron current which flows along the grain boundary, also shown in Fig. 2(a).

We note that the pinning of the electron quasi-Fermi level to  $E_{\text{GB}}$  results in a constant electron density along the grain boundary ( $n_{\text{GB}} \approx \bar{n}_{\text{GB}}$ ). Therefore the electron current has only a drift component. The driving force for the drift current is an electrostatic potential that develops along the grain boundary. For low currents, the electrostatic field and associated electrostatic potential gradient is small and can be neglected. The red curves of Fig. 3(a) and (b) respectively show that the electrostatic potential and hole density are constant along the grain boundary in this case. The red curve of Fig. 3(c) shows the electron current along the grain boundary; the spatially constant hole density and recombination leads to a linearly increasing electron current (consistent with the picture of Fig. 2(a)).

Using Eq. (9) and the assumption of flat hole quasi-Fermi level, Fig. 2(d) shows that the distance between  $E_{F_p}$  and the valence band is  $E_{\text{GB}} - qV$ ; the grain bound-

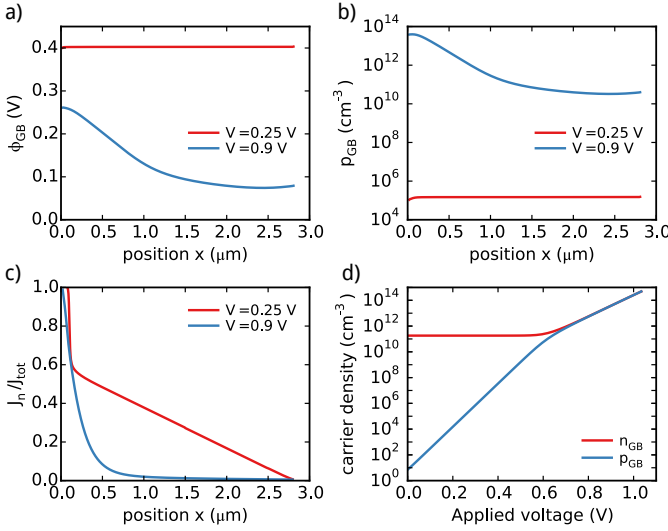


FIG. 3. (a) Electrostatic potential along the grain boundary. (b) grain boundary hole density along the grain boundary. (c) Electron current in the  $x$ -direction normalized by the total current, both currents are integrated in the  $y$ -direction. (d) grain boundary electron (red) and hole (blue) densities in the depletion region as a function of applied voltage. For (a), (b) and (c) red corresponds to  $V = 0.25$  V and blue corresponds to  $V = 0.9$  V. All simulations were done for  $S_n = S_p = 10^5$  cm/s,  $\mu_e = \mu_h = 100$   $\text{cm}^2/(\text{V} \cdot \text{s})$ ,  $E_{GB} = 1.1$  eV and  $N_A = 10^{16}$   $\text{cm}^{-3}$ . General parameters are listed in Table II.

ary hole density therefore reads

$$p_{GB} = N_V e^{(-E_{GB} + qV)/k_B T}. \quad (10)$$

Because  $S_n n_{GB} \gg S_p p_{GB}$  the grain boundary recombination is determined by the minority carrier  $p_{GB}$ , and is given by

$$R_{GB} = \frac{S_p}{2} p_{GB}. \quad (11)$$

The recombination is constant along the grain boundary, so the dark current of Eq. (7) simplifies to

$$J_{GB}(V) = \frac{S_p L_{GB} N_V}{2d} e^{(-E_{GB} + qV)/k_B T}. \quad (12)$$

The important features of Eq. (12) are: the saturation current varies as  $S_p L_{GB}/2d$ , the ideality factor is 1, and the thermal activation energy is  $E_{GB}$ .

In Appendix B, we derive and discuss the condition under which the hole quasi-Fermi level is approximately flat, given below ( $V_T = k_B T/q$ )

$$\frac{S_p}{4\mu_h} \sqrt{\frac{2\epsilon}{qV_T N_A}} < 1. \quad (13)$$

For  $S_n = S_p = 10^5$  cm/s,  $N_A = 10^{15}$   $\text{cm}^{-3}$ ,  $\epsilon = 9.4 \epsilon_0$ , Eq. (13) is satisfied for  $\mu_h > 16$   $\text{cm}^2/(\text{V} \cdot \text{s})$ .

## B. Grain boundary recombination for $S_n n_{GB} \approx S_p p_{GB}$

As the applied voltage increases,  $S_p p_{GB}$  increases exponentially (see Eq. (10)), and eventually approaches  $S_n n_{GB}$ . Beyond this point,  $S_n n_{GB} \approx S_p p_{GB}$  and the previous analysis no longer applies. Fig. 3(d) shows the grain boundary electron and hole density at a point in the  $pn$  junction depletion region versus the applied voltage.  $V = 0.7$  V delineates the  $S_n n_{GB} \gg S_p p_{GB}$  and  $S_n n_{GB} \approx S_p p_{GB}$  regimes. To proceed in the  $S_n n_{GB} \approx S_p p_{GB}$  case, we start with the general form of the carrier densities along the grain boundary. Using the energy scale and definitions of Fig. 1(b), the densities are

$$n_{GB}(x) = N_C e^{(E_{F_n}(x) + q\phi_{GB}(x) - E_g)/k_B T} \quad (14)$$

$$p_{GB}(x) = N_V e^{(-E_{F_p} - q\phi_{GB}(x))/k_B T}, \quad (15)$$

where  $\phi_{GB}(x)$  is the electrostatic potential at the grain boundary. (Note that  $\phi_{GB}(x) = V_{GB}$  for  $x$  in the neutral region. However when  $S_n n_{GB} \approx S_p p_{GB}$ , the electron quasi-Fermi level is not pinned to  $E_{GB}$  and  $V_{GB}$  is not known.)

Since  $S_n n_{GB} \approx S_p p_{GB}$ , we can equate Eqs. (14) and (15) to obtain

$$E_{F_n}(x) = -2q\phi_{GB}(x) - E_F - E_g - k_B T \ln \left( \frac{S_n N_C}{S_p N_V} \right), \quad (16)$$

where we assumed  $E_{F_p} = E_F$ <sup>24</sup>. Using the continuity equation and the selective contacts boundary conditions, we show in Appendix C that  $E_{F_n}$  obeys

$$E_{F_n}(x) = -k_B T \sqrt{\frac{S}{D_e W}} x + E_F + qV, \quad (17)$$

where

$$W = \sqrt{2\pi\epsilon V_T / (qN_A)} \quad (18)$$

is the width across the grain boundary over which the electron current is confined (see Appendix C),  $D_e = k_B T \mu_e / q$  is the electron diffusion constant ( $\mu_e$ : electron mobility), and  $S = \sqrt{S_n S_p}$  is an effective surface recombination velocity. The electrostatic potential along the grain boundary is found with Eqs. (17)-(16):

$$\phi_{GB}(x) = \frac{V_T}{2} \sqrt{\frac{S}{D_e W}} x - \frac{V}{2} - V_T \ln(n_i / N_V). \quad (19)$$

We observe that both  $\phi_{GB}(x)$  and  $E_{F_n}(x)$  vary linearly along the length of the grain boundary, and that their slopes differ by a factor of 2. The blue curve of Fig. 3(a) shows that the numerically computed electrostatic potential along the grain boundary is approximately linear near the  $pn$  junction<sup>25</sup>.

Given the electrostatic potential of the grain boundary, we use the assumption of flat hole quasi-Fermi level to evaluate the grain boundary hole density. Using Eqs. (15) and (19), we obtain:

$$p_{GB}(x) = n_i e^{V/(2V_T)} e^{-\sqrt{\frac{S}{D_e W}} \frac{x}{2}}. \quad (20)$$

The important feature of Eq. (20) is that the hole density varies along the grain boundary, which we will discuss in more detail below. Because we assumed  $S_n n_{\text{GB}} \approx S_p p_{\text{GB}}$ , the grain boundary recombination is still given by Eq. (11). Integrating the hole density over the length of the grain boundary leads to

$$J_{\text{GB}}(V) = \frac{n_i \sqrt{SD_e W}}{d} e^{V/(2V_T)} \times \left[ 1 - e^{-\sqrt{\frac{S}{D_e W}} \frac{L_{\text{GB}}}{2}} \right]. \quad (21)$$

Equation (21) is the general result for the grain boundary recombination current in the case  $S_n n_{\text{GB}} \approx S_p p_{\text{GB}}$ . Note that our analysis assumes that the total current at  $x = 0$  is equal to the electron current, or equivalently, that the hole current along the grain boundary is negligible. Generally the limiting cases we observe are that the total current at  $x = 0$  is either all electron current, or equal parts electron and hole current. Our assumption of all electron current at  $x = 0$  can therefore overestimate the grain boundary recombination current by a maximum factor of 2.

Equation (21) is best understood in two limiting cases. In the first limit, the potential drop across the length of grain boundary is much less than  $V_T$ . Using Eq. (19), this is written as

$$\frac{\phi_{\text{GB}}(L_{\text{GB}}) - \phi_{\text{GB}}(0)}{V_T} = \sqrt{\frac{S}{D_e W}} \frac{L_{\text{GB}}}{2} \ll 1. \quad (22)$$

This indicates that the argument of the exponential term in brackets in Eq. (21) is small. Expanding in this small parameter leads to

$$J_{\text{GB}}(V) = \frac{SL_{\text{GB}}}{2d} n_i e^{V/(2V_T)}. \quad (23)$$

Results similar to Eq. (23) are available in previous work<sup>20</sup>. Because the electrostatic potential difference along the grain boundary is negligible, the picture of a uniform grain boundary described in the previous section, as well as the description of current flow given in Fig. 2(a) apply in this case. We refer to these cases as “linear” regimes because the recombination current is linear in surface recombination velocity (see Eq. (12) and Eq. (23)). In this  $S_n n_{\text{GB}} \approx S_p p_{\text{GB}}$  case, the thermal activation energy is  $E_g/2$  and the ideality factor is 2. Previous experimental work which aimed to isolate the grain boundary recombination current in Si  $pn^+$  junctions observed such a thermal activation energy and ideality factor<sup>26</sup>. The crossover between  $S_n n_{\text{GB}} \gg S_p p_{\text{GB}}$  and  $S_n n_{\text{GB}} \approx S_p p_{\text{GB}}$  regimes occurs at an applied voltage  $V_{c1}$  which is determined by equating Eqs. (12) and (23), yielding

$$qV_{c1} = 2E_{\text{GB}} - E_g + k_B T \ln \left( \frac{S_n N_C}{S_p N_V} \right). \quad (24)$$

The second limit of Eq. (21) occurs when the potential

drop along the grain boundary is much greater than  $V_T$

$$\frac{\phi_{\text{GB}}(L_{\text{GB}}) - \phi_{\text{GB}}(0)}{V_T} = \sqrt{\frac{S}{D_e W}} \frac{L_{\text{GB}}}{2} \gg 1. \quad (25)$$

In this case the exponential term in brackets in Eq. (21) is negligible, leading to

$$J_{\text{GB}}(V) = \frac{n_i \sqrt{SD_e W}}{d} e^{V/(2V_T)}. \quad (26)$$

The physical picture associated with this case is shown in Fig. 2(b): hole currents are now directed toward the grain boundary in the  $pn$  junction depletion region, where holes recombine and generate an electron current mainly concentrated there. The recombination occurs primarily at this “hotspot” in the depletion region, in similar fashion (although with important differences) to previous studies of grain boundary recombination<sup>21</sup>. We refer to this case as the “hotspot” regime.

In this limit, the steep drop in the potential along the grain boundary, combined with the flat hole quasi-Fermi level results in a grain boundary hole density (and ensuing recombination) which decays exponentially along the grain boundary. The blue curve of Fig. 3(b) shows this behavior. From the continuity equation, the exponential decay of the recombination implies that the electron current along the grain boundary also decays exponentially from the carrier density hotspot, supporting the description of Fig. 2(c).

The form of Eq. (26) is quite peculiar; the saturation current density is proportional to  $\sqrt{SD_e W}$ , which has some similarities to the conventional form for diffusive recombination saturation current, such as a saturation current density which scales as  $\sqrt{D_e}$ . But the ideality factor of 2 and thermal activation energy of  $E_g/2$  are typical of junction recombination. The crossover with the regime  $S_n n_{\text{GB}} \gg S_p p_{\text{GB}}$  occurs at an applied voltage

$S_n n_{\text{GB}} \gg S_p p_{\text{GB}}$
$J_{\text{GB}}(V) = \frac{S_p L_{\text{GB}} N_V}{2d} e^{(-E_{\text{GB}} + qV)/k_B T}$
$S_n n_{\text{GB}} \approx S_p p_{\text{GB}}$
$J_{\text{GB}}(V) = \frac{n_i \sqrt{SD_e W}}{d} e^{V/(2V_T)} \left[ 1 - e^{-\sqrt{\frac{S}{D_e W}} \frac{L_{\text{GB}}}{2}} \right]$
$\approx \frac{n_i SL_{\text{GB}}}{2d} e^{V/(2V_T)} \quad \text{for } \sqrt{\frac{S}{D_e W}} \frac{L_{\text{GB}}}{2} \ll 1$
$\approx \frac{n_i \sqrt{SD_e W}}{d} e^{V/(2V_T)} \quad \text{for } \sqrt{\frac{S}{D_e W}} \frac{L_{\text{GB}}}{2} \gg 1$

TABLE I. Summary of the analytical results for the grain boundary recombination current derived in Sec. III.  $S_n, p$ ,  $E_{\text{GB}}$ ,  $L_{\text{GB}}$  are the grain boundary recombination velocity, defect level energy, and length, respectively.  $S = \sqrt{S_n S_p}$ ,  $W = \sqrt{2\pi\epsilon V_T / (qN_A)}$ ,  $D_e$  is the electron diffusivity at the grain boundary, and  $d$  is the grain size.

$V_{c2}$ , which is determined by equating the recombination currents in both cases (Eqs. (12) and (26)), yielding

$$qV_{c2} = 2E_{GB} - E_g + k_B T \ln \left( 4 \frac{N_C}{N_V} \sqrt{\frac{S_n D_e W}{S_p^3 L_{GB}^2}} \right). \quad (27)$$

For  $\mu_{e,h} = 300 \text{ cm}^2/(\text{V} \cdot \text{s})$ ,  $N_A = 10^{15} \text{ cm}^{-3}$  and  $L_{GB} = 3 \text{ } \mu\text{m}$ , the system is in the hotspot (linear) regime for  $S_{n,p}$  greater (smaller) than  $10^4 \text{ cm/s}$ . We again determine the conditions under which the assumption of a flat hole quasi-Fermi level is valid, which we quote here and derive in Appendix B

$$\frac{S_p}{8\mu_h} \sqrt{\frac{2\epsilon}{qV_T N_A}} < 1. \quad (28)$$

The analytical results of this section are summarized in Table I.

### C. Numerical calculations

We perform numerical simulations of the drift-diffusion-Poisson equations for the geometry presented in Fig. 1(a) to test the accuracy of the above results. Table II gives the list of material parameters used for these calculations. We used infinite (zero) surface recombination velocities for majority (minority) carriers at the contacts, and periodic boundary conditions in the  $y$ -direction.

In Fig. 4(a) the doping density is varied from  $10^{14} \text{ cm}^{-3}$  to  $10^{16} \text{ cm}^{-3}$  for  $E_{GB} = 1.1 \text{ eV}$ . For  $V < V_{c2}$  the system is in the linear regime  $S_n n_{GB} \gg S_p p_{GB}$  and the grain boundary recombination current is independent of  $N_A$  as predicted by Eq. (12). Upon increasing  $V$  above  $V_{c2}$ , the system switches to the hotspot regime given by Eq. (26), as can be seen by the change of slope of the current. The grain boundary recombination currents now depend on the doping density and do not overlap. The predicted scaling in  $N_A^{-1/4}$  is verified in the inset.

We show the dependence of the grain boundary recombination current on the defect energy level  $E_{GB}$  in Fig. 4(b). For applied voltages below 1 V, the grain boundary with  $E_{GB} = 1.35 \text{ eV}$  remains in the linear regime  $S_n n_{GB} \gg S_p p_{GB}$ , while for  $E_{GB} = 0.75 \text{ eV}$  the grain boundary is always in the hotspot configuration as seen by the absence of slope change. The crossover between these regimes in the case  $E_{GB} = 1.1 \text{ eV}$  confirms the independence of Eq. (26) of the grain boundary defect energy level. In addition, a comparison of the magnitudes of the recombination currents indicates that a higher defect energy level is favorable for reduced grain boundary recombination. This will impact the open-circuit voltage significantly, as will be discussed in Sec. V.

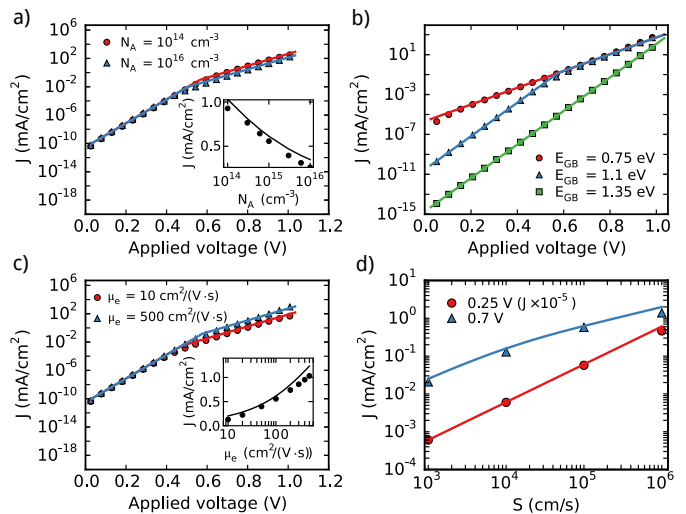


FIG. 4. grain boundary recombination current characteristics  $J_{GB}(V)$  for  $E_{GB} = 1.1 \text{ eV}$  and  $S_n = S_p = 10^5 \text{ cm/s}$  unless specified otherwise. Symbols are numerical calculations, full lines correspond to analytical results Eqs. (12) and (21). (a)  $\mu_e = 100 \text{ cm}^2/(\text{V} \cdot \text{s})$ . Inset: grain boundary recombination current as a function of doping density at  $V = 0.7 \text{ V}$ . (b)  $\mu_e = 500 \text{ cm}^2/(\text{V} \cdot \text{s})$ ,  $N_A = 10^{15} \text{ cm}^{-3}$ . (c)  $N_A = 10^{15} \text{ cm}^{-3}$ . Inset: grain boundary recombination current as a function of electron mobility for  $V = 0.7 \text{ V}$ . (d) grain boundary recombination current as a function of surface recombination velocity ( $S_n = S_p$ ), at  $V = 0.25 \text{ V}$  (dots) and  $V = 0.7 \text{ V}$  (triangles).  $\mu_e = 100 \text{ cm}^2/(\text{V} \cdot \text{s})$ ,  $N_A = 10^{15} \text{ cm}^{-3}$ .

We vary the mobility of carriers (taken equal for electrons and holes) in Fig. 4(c) for  $E_{GB} = 1.1 \text{ eV}$ . As predicted by Eq. (12) the linear regime is independent of mobility. The dependence of the hotspot regime on mobility is seen for  $V > V_{c2}$ , and we check the predicted square root scaling in the inset. The grain boundary recombination current is increased as carrier mobility is increased. Increasing carrier mobility means that the gradient in electrostatic potential needed to drive the current is reduced (see Eq. (19)). This in turn results in less suppression of hole density away from the hotspot, and an increase in the total grain boundary recombination. We also note that the electron mobility at the grain boundary controls the recombination. We have checked that changing the bulk electron mobility has no effect on the grain boundary recombination. A similar observation was made in Ref. 27.

Our last test is in Fig. 4(d); we show grain boundary recombination currents in both regimes,  $S_n n_{GB} \gg S_p p_{GB}$  and  $S_n n_{GB} \approx S_p p_{GB}$ , as a function of surface recombination velocity. The analytical predictions are in good agreement with the numerical calculations, and we verify the  $\sqrt{S}$  dependence of the grain boundary recombination current for  $V > V_{c2}$ . This dependence only applies for  $S > 10^4 \text{ cm/s}$ ; for lower values of  $S$ , the system crosses over between the hotspot and the linear configuration of the  $S_n n_{GB} \approx S_p p_{GB}$  regime.

Finally, we verified numerically that multiple paral-

Parameter	Value
$L$	$3 \mu\text{m}$
$d$	$5 \mu\text{m}$
$N_C$	$8 \times 10^{17} \text{ cm}^{-3}$
$N_V$	$1.8 \times 10^{19} \text{ cm}^{-3}$
$E_g$	$1.5 \text{ eV}$
$N_A$	$10^{14} \text{ cm}^{-3}$ to $10^{16} \text{ cm}^{-3}$
$N_D$	$10^{17} \text{ cm}^{-3}$
$\mu_e = \mu_h$	$1 \text{ cm}^2/(\text{V} \cdot \text{s})$ to $500 \text{ cm}^2/(\text{V} \cdot \text{s})$
$\epsilon$	$9.4 \epsilon_0$
$\tau_e = \tau_h$	$10 \text{ ns}$
$S_{n,p}$	$10^3 \text{ cm/s}$ to $10^6 \text{ cm/s}$
$\rho_{\text{GB}}$	$10^{14} \text{ cm}^{-2}$

TABLE II. List of default parameters for numerical simulations.

el grain boundaries contribute independently to the recombination current. The total grain boundary recombination current is therefore the sum of individual grain boundary recombination currents, so that the formulas derived here can be readily applied to systems with non-uniform distribution of grain boundary properties. Because of the independence of grain boundary recombination, the geometry of our model is easily generalized. Our model consists of periodic grains parallel to the  $x-z$  plane separated by a distance  $d$ . For a system composed of grains with square sections of side length  $d$ , the grain boundary 2D density doubles so that the distance  $d$  present in the expressions of the paper should be changed to  $d/2$  (assuming no additional complexity due to intersections of grain boundaries).

#### IV. BULK RECOMBINATION OF THE SYSTEM

We now turn to the bulk recombination of the system. This comprises the recombination current from the  $pn$  junction depletion region, and the grain interior neutral and depletion regions.

The  $pn$  junction recombination current is taken from the standard 1D model of a  $pn$  junction<sup>28</sup>, and assumed uniform across the system

$$J_{pn}(V) = W_{\text{eff}} \frac{n_i}{2\tau_e} e^{V/(2V_T)}, \quad (29)$$

where  $W_{\text{eff}}$  is a fraction of the  $pn$  junction depletion region width and  $\tau_e$  is the electron lifetime.

The behavior of the grain interior depletion region depends on the carrier densities at the grain boundary. In the linear regime, the majority carrier type of the grain boundary is inverted compared with the grain interior, which results in the crossing of the carrier densities in the grain interior depletion region. The recombination profile is therefore peaked with the same analytical expression as that of the  $pn$  junction depletion region. We suppose the recombination is uniform along the grain boundary, so

that the integration along both sides of the grain boundary yields the recombination current

$$J_{\text{GI}}^{\text{depl}}(V) = W'_{\text{eff}} \frac{n_i}{2\tau_e} e^{V/(2V_T)} \times \frac{2L_{\text{GB}}}{d}, \quad (30)$$

where  $W'_{\text{eff}}$  is a fraction of the width of the grain interior depletion region. The upper inset of Fig. 5 shows that in the linear regime, the bulk recombination along the grain boundary has the same magnitude as that of the  $pn$  junction depletion region, hence cannot be neglected. However, in the hotspot regime the grain boundary is not inverted. As a result, the carrier densities profiles do not cross in the grain interior depletion region, which significantly reduces the bulk recombination. The lower inset of Fig. 5 shows that the bulk recombination of the system is now dominated by the  $pn$  junction depletion region, and the grain interior depletion region recombination can be neglected.

We now turn to the recombination in the neutral region of the grain interior which is determined by the electron density there. We assume that the electron density is uniform in the  $y$ -direction which allows us to reduce the 2-dimensional problem to a 1-dimensional one. This electron density therefore satisfies the diffusion equation

$$\frac{d^2 n}{dx^2} - \frac{n}{L_e^2} = 0, \quad (31)$$

where  $L_e = \sqrt{D_e \tau_e}$  is the electron diffusion length, with the boundary conditions ( $W_p$ : depletion region width,  $L$ :

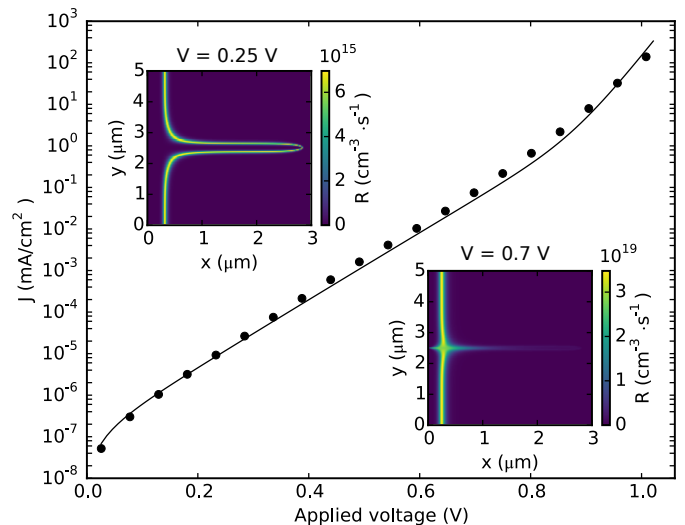


FIG. 5. Bulk recombination current of the system. Dots are numerical data of the integration over the entire system of the bulk recombination only (no grain boundary recombination), the continuous line corresponds to the sum of Eqs. (29), (30) and (35). Parameters:  $N_A = 10^{15} \text{ cm}^{-3}$ ,  $E_{\text{GB}} = 1.1 \text{ eV}$ ,  $\mu_e = 100 \text{ cm}^2/(\text{V} \cdot \text{s})$ ,  $S_n = S_p = 10^5 \text{ cm/s}$ . The lifetime of electrons and holes is 10 ns. Insets: Color maps of the bulk recombination for  $V = 0.25 \text{ V}$  (upper), and  $V = 0.7 \text{ V}$  (lower).

distance between the contacts)

$$n(W_p) = \frac{n_i^2}{N_A} e^{V/V_T} \text{ and } \frac{dn}{dx}(L) = 0. \quad (32)$$

The second boundary condition is imposed by our assumption of zero electron current at  $x = L$  (selective contact). The solution to Eq. (31) reads

$$n(x) = \frac{n_i^2}{N_A} e^{V/V_T} \frac{\cosh\left(\frac{L-x}{L_e}\right)}{\cosh\left(\frac{L-W_p}{L_e}\right)}. \quad (33)$$

The recombination current from the grain interior neutral region for  $V > V_T$  (neglecting the term in  $n_i^2$ ) is given by

$$J_{\text{GI}}^{\text{neut}}(V) = \frac{d'}{d\tau_e} \int_{W_p}^L dx \frac{np}{n+p}, \quad (34)$$

where  $p = N_A$  and  $d'$  is a fraction of the width of the system which represents the extent of the grain interior neutral region. For doping densities above  $5 \times 10^{14} \text{ cm}^{-3}$  and applied voltages below 0.9 V, one has  $n \ll N_A$  so that Eq. (34) reduces to the integral of the electron density Eq. (33) over the neutral region. The contribution of the neutral domain of the grain interior hence reads

$$J_{\text{GI}}^{\text{neut}}(V) = \sqrt{\frac{D_e}{\tau_e}} \frac{n_i^2}{N_A} e^{V/V_T} \tanh\left(\frac{L-W_p}{L_e}\right) \times \frac{d'}{d}. \quad (35)$$

The exact calculation of Eq. (34) is in Appendix D.

Figure 5 shows good agreement between the sum of the analytical results Eqs. (29), (30) and (35) and the numerically computed bulk recombination current. The recombination is mainly dominated by the depletion regions until  $V \approx 0.8$  V, where the contribution of the diffusive current in the neutral region is observed as the ideality factor changes from 2 to 1. While the grain boundary recombination dominates over bulk for large surface recombination velocities, bulk recombination must be accounted for to determine  $V_{\text{oc}}$  accurately for small values of  $S_{n,p}$ . This is shown in Fig. 6(b);  $V_{\text{oc}}$  is independent of  $S_{n,p}$  for  $S_{n,p} < 10^3 \text{ cm/s}$  and is now approximated by the sum of Eqs. (29), (30) and (35) taken equal to the numerically determined short-circuit current.

## V. OPEN-CIRCUIT VOLTAGE

We next consider the impact of charged grain boundaries on the open-circuit potential  $V_{\text{oc}}$  of the system under illumination. For realistic/large surface recombination velocities, grain boundaries dominate the dark current. In this case, simple analytic forms for the open-circuit voltage are summarized in Table III.

If the current-voltage relation under illumination is given by the sum of the short circuit current density  $J_{\text{sc}}$

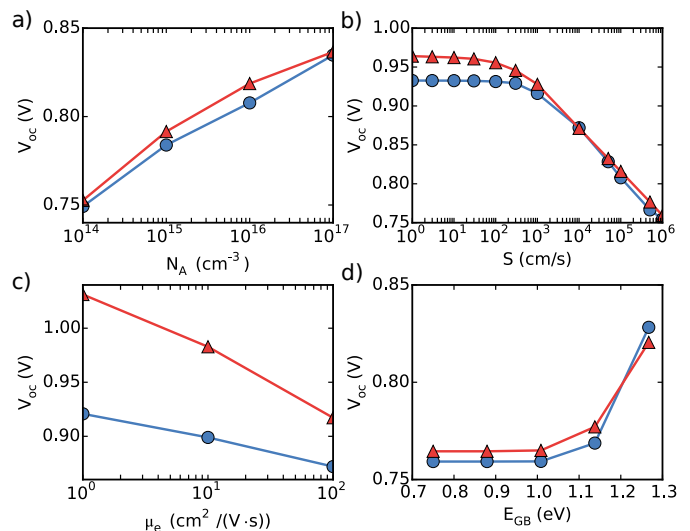


FIG. 6. Open circuit voltage for our system described in Fig. 1(a) under a photon flux  $10^{21} \text{ m}^{-2} \cdot \text{s}^{-1}$ . The absorption length is  $2.3 \times 10^4 \text{ cm}^{-1}$  and  $E_{\text{GB}} = 1.1 \text{ eV}$ . The carriers mobility is  $100 \text{ cm}^2/(\text{V} \cdot \text{s})$ ,  $N_A = 10^{16} \text{ cm}^{-3}$  and  $S_n = S_p$  unless specified otherwise.  $N_D = 10^{19} \text{ cm}^{-3}$ . Numerical data are in blue (dots) and analytical predictions are in red (triangles). (a)  $V_{\text{oc}}$  as a function of doping density,  $S_{n,p} = 10^5 \text{ cm/s}$ . (b)  $V_{\text{oc}}$  as a function of surface recombination velocity. (c)  $V_{\text{oc}}$  as a function of electron and hole mobility (assumed equal) for  $S_{n,p} = 10^4 \text{ cm/s}$ . (d)  $V_{\text{oc}}$  as a function of grain boundary defect energy level for  $S_{n,p} = 10^5 \text{ cm/s}$ .

and the dark  $J(V)$  (a condition known as the superposition principle), then  $V_{\text{oc}}$  satisfies  $J(V_{\text{oc}}) = J_{\text{sc}}$ . The applicability of the superposition principle in this system is not clear *a priori*. Indeed, photogenerated carriers can modify the occupancy and charge of the grain boundary defect level. This in turn alters the electrostatics of the problem, so that the models of Sec. III may no longer apply. Empirically, we find that the superposition principle is not particularly reliable for lower applied voltages (lower than  $V_{c1}$ ,  $V_{c2}$ ). However, for applied voltages near  $V_{\text{oc}}$  we find that the superposition principle is approximately satisfied. Figure 6 shows the numerically computed  $V_{\text{oc}}$  for the system under illumination, compared to the  $V_{\text{oc}}$  predicted using the numerically computed  $J_{\text{sc}}$  and the analytic forms for  $J(V)$ .

Assuming large values of surface recombination velocities, therefore neglecting the bulk recombination, we can write down explicit forms for the open-circuit voltage associated with the dark grain boundary recombination current. As before, there are several distinct cases. The appropriate form of  $J(V)$  to use in solving  $J(V_{\text{oc}}) = J_{\text{sc}}$  depends on the value of  $\sqrt{\frac{S}{D_e W}} \frac{L_{\text{GB}}}{2}$  and  $J_{\text{sc}}$ . For example, if  $\sqrt{\frac{S}{D_e W}} \frac{L_{\text{GB}}}{2} \gg 1$ , then at an applied voltage  $V_{c2}$  the system goes from the linear regime of Eq. (12) to the hotspot regime of Eq. (26). If  $J(V_{c2})$  is greater than  $J_{\text{sc}}$ , then Eq. (26) is used to solve  $J(V_{\text{oc}}) = J_{\text{sc}}$  for  $V_{\text{oc}}$ . Otherwise Eq. (12) is used to determine  $V_{\text{oc}}$ . All the ex-

$\sqrt{\frac{S}{D_e W}} \frac{L_{GB}}{2} \ll 1$	
$V_{oc}^{GB} =$	$\begin{cases} E_g/q + 2V_T \ln\left(\frac{2J_{sc}d}{\sqrt{N_C N_V} S L_{GB}}\right) & \text{for } J_{sc} > J(V_{c1}) \\ E_{GB}/q + V_T \ln\left(\frac{2J_{sc}d}{N_V S_p L_{GB}}\right) & \text{for } J_{sc} < J(V_{c1}) \end{cases}$
$\sqrt{\frac{S}{D_e W}} \frac{L_{GB}}{2} \gg 1$	
$V_{oc}^{GB} =$	$\begin{cases} E_g/q + 2V_T \ln\left(\frac{J_{sc}d}{\sqrt{N_C N_V} S}\right) & \text{for } J_{sc} > J(V_{c2}) \\ E_{GB}/q + V_T \ln\left(\frac{2J_{sc}d}{N_V S_p L_{GB}}\right) & \text{for } J_{sc} < J(V_{c2}) \end{cases}$

TABLE III. Summary of the analytical results for the open circuit voltage associated with grain boundary recombination current derived in Sec. III. The critical voltages  $V_{c1}$  and  $V_{c2}$  are given in Eqs. (24) and (27), respectively.

pressions with their domains of applicability are given in Table III for the various cases.

The results of Table III provide insight into the precise role of grain boundaries in determining  $V_{oc}$ . For example, in all cases we consider,  $V_{oc}$  decreases logarithmically with the grain size  $d$ . For the hotspot case,  $V_{oc}$  is independent of grain boundary defect energy level, seen in the saturation of  $V_{oc}$  for  $E_{GB} < 1.1$  eV in Fig. 6(d), and grain boundary length in the  $x$ -direction. On the contrary,  $V_{oc}$  increases linearly with the grain boundary defect energy level in the linear regime, which implies that higher defect energy levels increase the open-circuit voltage in this case. Interestingly, in the hotspot regime,  $V_{oc}$  is increased with decreasing electron mobility (Fig. 6(c)). This is because a stronger electrostatic potential drop along the grain boundary is required to drive the current for lower electron mobility, and this leads to more suppression of hole density and recombination.

In Fig. 6(b), we reduce  $S_{n,p}$  to values which correspond to capture cross sections  $\sigma_{n,p}$  which are unphysical (given the assumption of high  $\rho_{GB}$ ). However, we present these results for the purposes of validating the mathematical analysis of the model. We note that for small enough  $S_{n,p}$ , bulk recombination dominates. More precisely, the  $pn$  junction depletion region and the neutral grain interior determine  $V_{oc}$ . Indeed, for the grain boundary energy level  $E_{GB} = 1.1$  eV presented here, the grain boundary is in the hotspot regime for  $V \approx V_{oc}$  and the recombination of the grain interior depletion region is negligible (see insets of Fig. 5).

## VI. CONCLUSION

This work investigates the influence of grain boundaries on the efficiency of polycrystalline thin films solar cells. To this end we derived analytic expressions for the grain boundary dark recombination current and provided physical pictures for the charge carrier trans-

port, both supported by numerical simulations. Within reasonable approximations we found that our analytic results give the proper functional dependence of the grain boundary recombination current on the parameters  $V$ ,  $S_{n,p}$ ,  $E_{GB}$ ,  $N_A$ ,  $\mu_{e,h}$ ,  $L_{GB}$ ,  $L$ ,  $d$ ,  $\tau_{e,h}$  and  $E_g$ . We showed that for realistic surface recombination velocities, the grain boundary recombination dominates over the bulk recombination, and reduces the open circuit voltage. We believe the physical pictures of charged grain boundaries, and the corresponding analytic results given here are not limited to CdTe and Cu(In, Ga)Se<sub>2</sub>. Other materials such as polycrystalline Si, and GaAs bicrystals<sup>29</sup> exhibit grain boundary built-in potentials of several hundred mV. Our analysis could be extended to these materials as well.

## ACKNOWLEDGMENTS

B. G. acknowledges support under the Cooperative Research Agreement between the University of Maryland and the National Institute of Standards and Technology Center for Nanoscale Science and Technology, Award 70NANB10H193, through the University of Maryland.

## Appendix A CONDITION FOR FERMIL LEVEL PINNING AT GRAIN BOUNDARY DEFECT ENERGY LEVEL

We derive the critical defect density Eq. (5) that sets the pinning of the Fermi level to the grain boundary defect energy level. We consider the grain boundary at thermal equilibrium in the neutral region of  $pn$  junction. The grain boundary electron and hole densities are related to their grain interior counterparts by the grain boundary built-in potential  $V_{GB}$ ,

$$n_{GB} = \frac{n_i^2}{N_A} e^{V_{GB}/V_T} \quad (36)$$

$$p_{GB} = N_A e^{-V_{GB}/V_T}, \quad (37)$$

where  $N_A$  is the acceptor density, and  $V_T = k_B T/q$ . We assume the grain boundary core to be  $n$ -type so that  $S_p \bar{p}_{GB}$  and  $S_p p_{GB}$  are negligible. We define the difference between  $E_{GB}$  and  $E_F$ ,  $\delta E$ , which we will assume small compared to  $k_B T$ :  $E_F + \delta E = E_{GB} - qV_{GB}$ , to rewrite Eq. (1) as

$$Q_{GB} = q \frac{\rho_{GB}}{2} \left( 1 - \frac{2}{1 + \exp(\delta E/k_B T)} \right). \quad (38)$$

Using a depletion approximation and  $\delta E \ll E_{GB} - E_F$ , the charge in the depleted regions surrounding the grain boundary is

$$Q = \sqrt{8\epsilon q N_A V_{GB}} \approx \sqrt{8\epsilon q N_A (E_{GB} - E_F)}. \quad (39)$$

We set the criterion  $\delta E = k_B T$  to have  $E_F$  close to the defect state, which yields the critical grain boundary de-

fect density of states

$$\rho_{GB}^{crit} = \frac{2}{q} \left( \frac{e+1}{e-1} \right) \sqrt{8q\epsilon N_A (E_{GB} - E_F)}. \quad (40)$$

We restrict the scope of this paper to defect densities larger than  $\rho_{GB}^{crit}$ .

## Appendix B CONDITION FOR NEARLY FLAT HOLE QUASI-FERMI LEVEL

We specify the domain of validity of the assumption of flat hole quasi-Fermi level. In particular, we will consider  $E_{F_p} = E_F$  when variations of  $E_{F_p}$  across the grain boundary are smaller than  $k_B T$ . An expansion of  $E_{F_p}$  across the grain boundary yields

$$E_{F_p} = E_F - \left| \frac{\partial E_{F_p}}{\partial y} \right| \delta y, \quad (41)$$

where the gradient of  $E_{F_p}$  at the grain boundary depends on whether we consider the linear or hotspot regime.

For the linear regime, the gradient of  $E_{F_p}$  is obtained by integrating the continuity equation for holes across the grain boundary

$$\left| \frac{\partial E_{F_p}}{\partial y} \right| = q \frac{S_p}{4\mu_h}. \quad (42)$$

Assuming that the variation of  $E_{F_p}$  across the grain boundary follows that of the electrostatic potential, the distance across the grain boundary where  $E_F - E_{F_p} < k_B T$  is given by a depletion approximation  $\delta y = \sqrt{2\epsilon V_T / (qN_A)}$ . The assumption of flat  $E_{F_p}$  is therefore valid for

$$\frac{S_p}{4\mu_h} \sqrt{\frac{2\epsilon}{qV_T N_A}} < 1. \quad (43)$$

In the hotspot regime, the same approach is used but the continuity equation is considered at the hotspot across the entire  $y$ -direction. Because of the hotspot, the hole and electron currents integrated along the  $y$ -direction are equal to half the recombination current. The gradient of  $E_{F_p}$  across the grain boundary is therefore reduced by a factor 2

$$\left| \frac{\partial \phi_p}{\partial y} \right| = q \frac{S_p}{8\mu_h}, \quad (44)$$

which leads to the criterion

$$\frac{S_p}{8\mu_h} \sqrt{\frac{2\epsilon}{qV_T N_A}} < 1 \quad (45)$$

for the assumption of flat hole quasi-Fermi level to be valid.

## Appendix C DERIVATION OF EQ. (17)

We derive the electron quasi-Fermi level Eq. (17). We start with the most general expression of the product  $np$

$$np = n_i^2 e^{(E_{F_n} - E_{F_p}) / (k_B T)}. \quad (46)$$

Assuming  $S_n n_{GB} = S_p p_{GB}$ , the electron density at the grain boundary reads

$$n_{GB} = \sqrt{\frac{S_p}{S_n}} n_i e^{(E_{F_n} - E_{F_p}) / (2k_B T)}. \quad (47)$$

The electron current along the grain boundary is given by

$$J_n = W \mu_e n_{GB} \frac{\partial E_{F_n}}{\partial x}(x), \quad (48)$$

where  $W$  is a width which results from the spatial integral of the electron density transverse to the grain boundary, and is given by

$$W = \sqrt{\frac{2\pi\epsilon V_T}{qN_A}}. \quad (49)$$

Using Eq. (47) into Eq. (48) yields

$$J_n = W \mu_e \sqrt{\frac{S_p}{S_n}} n_i 2k_B T \frac{\partial}{\partial x} \left[ e^{(E_{F_n} - E_{F_p}) / (2k_B T)} \right]. \quad (50)$$

Neglecting the variation of the electron current transverse to the grain boundary, the continuity equation yields

$$W \mu_e \sqrt{\frac{S_p}{S_n}} n_i 2k_B T \frac{\partial^2}{\partial x^2} \left[ e^{(E_{F_n} - E_{F_p}) / (2k_B T)} \right] = q \frac{S_p}{2} n_i e^{(E_{F_n} - E_{F_p}) / (2k_B T)}, \quad (51)$$

which gives a second order differential equation for the exponential of the electron quasi-Fermi level

$$\frac{\partial^2}{\partial x^2} \left[ e^{E_{F_n} / (2k_B T)} \right] = \frac{\sqrt{S_n S_p}}{4D_e W} e^{E_{F_n} / (2k_B T)}, \quad (52)$$

where we used the fact that  $E_{F_p}$  is flat along the grain boundary, hence independent of  $x$ . Considering that  $E_{F_n} = E_F + qV$  at  $x = 0$  and that its spatial variation vanishes at  $x = L$  (no electron current in  $x = L$ ), we obtain

$$E_{F_n}(x) = E_F + qV - k_B T \sqrt{\frac{\sqrt{S_n S_p}}{D_e W}} x. \quad (53)$$

## Appendix D BULK DIFFUSIVE CURRENT EQ. (34)

Here we compute the integral Eq. (34) without assuming  $n \ll N_A$ . We obtained the following results

$$J_{GI}^{neut}(V) = d \frac{N_A L e}{\tau_e} \left[ \frac{L - W_p}{L_e} + \frac{2\alpha}{\sqrt{1 - \alpha^2}} \arctan \left( \frac{\alpha - 1}{\sqrt{1 - \alpha^2}} \tanh \left( \frac{L - W_p}{2L_e} \right) \right) \right] \quad (54)$$

for  $\alpha < 1$ ,

$$J_{\text{GI}}^{\text{neut}}(V) = d \frac{N_A L_e}{\tau_e} \left[ \frac{L - W_p}{L_e} + \frac{2\alpha}{\sqrt{\alpha^2 - 1}} \operatorname{artanh} \left( \frac{1 - \alpha}{\sqrt{\alpha^2 - 1}} \tanh \left( \frac{L - W_p}{2L_e} \right) \right) \right] \quad (55)$$

for  $\alpha > 1$ , and

$$J_{\text{GI}}^{\text{neut}}(V) = d \frac{N_A L_e}{\tau_e} \left[ \frac{L - W_p}{L_e} + \tanh \left( \frac{L - W_p}{2L_e} \right) \right] \quad (56)$$

for  $\alpha = 1$  with

$$\alpha = \frac{N_A^2 \cosh \left( \frac{L - W_p}{L_e} \right)}{n_i^2 e^{V/V_T}}. \quad (57)$$

<sup>1</sup>I. Dharmadasa, *Coatings* **4**, 282 (2014).

<sup>2</sup>S. G. Kumar and K. K. Rao, *Energy Environ. Sci.* **7**, 45 (2014).

<sup>3</sup>R. M. Geisthardt, M. Topič, and J. R. Sites, *IEEE J. Photovolt.* **5**, 1217 (2015).

<sup>4</sup>M. Topič, R. M. Geisthardt, and J. R. Sites, *IEEE J. Photovolt.* **5**, 360 (2015).

<sup>5</sup>H. P. Yoon, P. M. Haney, D. Ruzmetov, H. Xu, M. S. Leite, B. H. Hamadani, A. A. Talin, and N. B. Zhitenev, *Sol. Energ. Mat. Sol. Cells* **117**, 499 (2013).

<sup>6</sup>O. Zywitzki, T. Modes, H. Morgner, C. Metzner, B. Siepchen, B. Späth, C. Drost, V. Krishnakumar, and S. Frauenstein, *J. Appl. Phys.* **114**, 163518 (2013).

<sup>7</sup>C. Li, Y. Wu, J. Poplawsky, T. J. Pennycook, N. Paudel, W. Yin, S. J. Haigh, M. P. Oxley, A. R. Lupini, M. Al-Jassim, S. J. Pennycook, and Y. Yan, *Phys. Rev. Lett.* **112**, 156103 (2014).

<sup>8</sup>I. Visoly-Fisher, S. R. Cohen, and D. Cahen, *Appl. Phys. Lett.* **82**, 556 (2003).

<sup>9</sup>H. Moutinho, R. Dhere, C.-S. Jiang, Y. Yan, D. Albin, and M. Al-Jassim, *J. Appl. Phys.* **108**, 074503 (2010).

<sup>10</sup>C.-S. Jiang, R. Noufi, J. AbuShama, K. Ramanathan, H. Moutinho, J. Pankow, and M. Al-Jassim, *Appl. Phys. Lett.* **84**, 3477 (2004).

<sup>11</sup>M. Tuteja, P. Koirala, V. Palekis, S. MacLaren, C. S. Ferekides, R. W. Collins, and A. A. Rockett, *J. Phys. Chem. C* **120**, 7020 (2016).

<sup>12</sup>S. Sadewasser, D. Abou-Ras, D. Azulay, R. Baier, I. Balberg, D. Cahen, S. Cohen, K. Gartsman, K. Ganesan, J. Kavalakkatt, W. Li, O. Millo, T. Rissom, Y. Rosenwaks, H.-W. Schock, A. Schwarzman, and T. Unold, *Thin Solid Films* **519**, 7341 (2011).

<sup>13</sup>M. S. Leite, M. Abashin, H. J. Lezec, A. Gianfrancesco, A. A. Talin, and N. B. Zhitenev, *ACS Nano* **8**, 11883 (2014).

<sup>14</sup>S. Galloway, P. R. Edwards, and K. Durose, *Sol. Energ. Mat. Sol. Cells* **57**, 61 (1999).

<sup>15</sup>P. M. Haney, H. P. Yoon, B. Gaury, and N. B. Zhitenev, arXiv preprint arXiv:1605.04272 (2016).

<sup>16</sup>M. Gloeckler, J. R. Sites, and W. K. Metzger, *J. Appl. Phys.* **98**, 113704 (2005).

<sup>17</sup>K. Taretto and U. Rau, *J. Appl. Phys.* **103**, 094523 (2008).

<sup>18</sup>U. Rau, K. Taretto, and S. Siebentritt, *Appl. Phys. A* **96**, 221 (2009).

<sup>19</sup>F. Troni, R. Menozzi, E. Colegrove, and C. Buurma, *J. Electron. Mater.* **42**, 3175 (2013).

<sup>20</sup>J. G. Fossum and F. A. Lindholm, *IEEE Trans. Electron Devices* **27**, 692 (1980).

<sup>21</sup>M. A. Green, *J. Appl. Phys.* **80**, 1515 (1996).

<sup>22</sup>S. Edmiston, G. Heiser, A. Sproul, and M. Green, *J. Appl. Phys.* **80**, 6783 (1996).

<sup>23</sup>E. S. Yang, *Fundamentals of semiconductor devices* (McGraw-Hill Companies, 1978).

<sup>24</sup>The selective contact assumption implies that  $E_{F_p} = E_F$  at the  $p$ -contact, which is automatically extended to the entire system because of the assumption of flat hole quasi-Fermi level.

<sup>25</sup>We see that the numerically computed potential is not linear over the entire length of the grain boundary, however near the depletion region Eq. (19) gives a good approximation to the slope. This in turn accurately determines the decay of the hole density and the grain boundary recombination.

<sup>26</sup>A. Neugroschel and J. Mazer, *IEEE Trans. Electron Devices* **29**, 225 (1982).

<sup>27</sup>W. Metzger and M. Gloeckler, *J. Appl. Phys.* **98**, 063701 (2005).

<sup>28</sup>S. J. Fonash, *Solar cell device physics* (Academic Press, 1981).

<sup>29</sup>C. R. M. Grovenor, *J. Phys. C: Solid St. Phys.* **18**, 4079 (1985).